Analysis of Two-Dimensional Flow Fields in the Multi-Stage Turbomolecular Pump Using the DSMC Method

Joong-Sik Heo* and Young-Kyu Hwang**

Key words: Turbomolecular pump, Free molecular flow, Molecular transition region, Knudsen number, *Boltzmann equation, Monte Carlo method*

Abstract

The direct simulation Monte Carlo method is applied to investigate the two-dimensional flow fields of a turbomolecular pump (TMP) in both molecular and transition flow regions. The pumping characteristics of the TMP are investigated for a wide range of the Knudsen number. The maximum of compression ratio and of pumping speed strongly depend on the Knudsen number in transition region, while they weakly depend on the Knudsen number in free molecular flow region. The present numerical results show good agreement with the previously known experimental data. Finally, the results of the single blade row in both molecular and transition regions are used to predict the overall performance of a TMP, which has three kinds of blade with 24-rows.

Nomenclature

h : blade length [mm]
C_O : dimensionless blade-velocity ratio, $U_b/\sqrt{2RT}$
f : molecular velocity distribution function
K_{max} : maximum compression ratio
Kn : Knudsen number
L : characteristic length [mm]
N_{12} : number of molecules, see Eq. (6)
N_{21} : number of molecules, see Eq. (6)
N_1 : number of incident molecules, see Eq. (6)
N_{inlet} : number of molecules, see Eq. (5)
N_{outlet} : number of molecules, see Eq. (5)
P_{12} : probability, see Eq. (4)
P_{21} : probability, see Eq. (4)
P_1 : inlet pressure [Pa]
P_m : mean pressure, $(P_1+P_2)/2$
P_2 : outlet pressure [Pa]
R : ordinary gas constant [kJ/kg · K]
s : blade spacing [mm]
S_O : spacing-chord ratio($= s/h$)

* School of Mechanical Engineering, Sungkyunkwan University, Suwon, 440-746, Korea
** School of Mechanical Engineering, Sungkyunkwan University, Suwon, 440-746, Korea

t : time [sec]
T : absolute temperature [K]
U : bulk velocity of the molecules [m/s]
U_b : blade velocity [m/s]
v : random molecular velocity, see Eq. (1) [m/s]
w_{max} : dimensionless maximum pumping speed

Greek symbols

α : blade angle [degree]
λ : mean free path [mm]
τ : mean collision time [sec]

Subscripts

x, y, z : components in the $x-, y-, z-$ directions, respectively
1 : inlet side
2 : outlet side

Superscripts

t : at present time
Δt : time step

1. Introduction

Vacuum technology has been rapidly developed according to the variety of practical uses and the importance of industrial techniques. Turbomolecular pumps (TMP) are widely used for production of ultra high vacuum in many scientific and industrial applications. Advantages of the TMP are that it can produce cleaner and higher vacuum environment compared to an oil-diffusion pump and that since it does not use oil, the possibility of backstreaming of oil is removed. Furthermore, it reaches full operating speed within short periods after being switched on, and the lower power requirement produces a lower operating cost compared to a cryogenic pump.[1]

The mean free path lengths of gas particles are larger than the distance between the rotor blades in free molecular flow regions. Namely, the particles collide more frequently with blade surfaces than they collide with one another. So the blade velocity is effectively imposed on the gas particles as an additional component. The influence of moving blades on the gas particles is so significant in free molecular flow that the TMP has high volume flow rate and compression ratio. If an oil-free rotary pump is used as the fore-pump, the back-pressure of the TMP is about 1 Torr. In this case, collisions between molecules occur so frequently that the pumping performance becomes seriously poor. To enhance pumping throughput and operating pressure in molecular transition flow, various types of a TMP have been developed in many ways.[2] Recently, the compound molecular pump combining a molecular drag stage with the TMP was developed. This permitted discharge pressure between 10 and 20 Torr, making it possible to use three-stage diaphragm pumps.

Theoretical analyses of the parameters involved in the pumping action of the TMP have been well developed, and most of these works were fundamentally based on the free molecular flow assumptions. But, the flow in the later portion of stages (i.e., blade rows near the outlet) becomes molecular transition flows. To predict correctly the performance of the TMP, it is important to consider the collisions between molecules. A few researches were limited to the analyses for simple cases of a single blade row in the molecular transition flows. Sawada[3] studied the performance of the TMP in the transition region by using the Schaetzles relaxation techniques. The relaxation techniques have some difficulties in computation for large number of volume elements. Thus, the Knudsen number was limited about 1. Also, Sawada[4] studied theoretically and experimentally the

performance of the TMP, which has a single blade row, in the transition and slip flow regimes. In his study the following two assumptions are used: (1) uniformity of the molecular number density in the passage of a blade row and (2) equal division of molecules which collide with other molecules into inlet and outlet regions. But, these assumptions are incorrect in either the free- or near free-molecular flow region where the pressure ratio is high, as pointed out by Sawada.[4] Moreover, since the above studies are based on the kinetic theory of gases, it is not easy to solve the problems.

In this study, the direct simulation Monte Carlo (DSMC) method is applied to the flow analysis of the TMP blade rows. In order to predict the pumping performance in both molecular and transition flow regions, a new model, including the leakage through the clearance between rotor and stator, is developed. Also, the overall performance of the TMP through entire stages is calculated by using the single blade row results.

2. DSMC simulations

2.1 Single blade row and multi-stage calculations

The rotor of a TMP developed in the circumferential direction is shown in Fig. 1, where the rotor moves linearly with the dimensionless blade-velocity ratio C_O. This ratio is defined as $C_O = U_b/\sqrt{2RT}$, here U_b is the blade speed and $\sqrt{2RT}$ is the most probable molecular speed. As seen in Fig. 1, the x is the pumping direction and y is the circumferential direction.

The flow in the TMP blade rows is the free molecular or the transition region according to the back-pressure. This kind of flow can be only accurately described by the nonlinear Boltzmann equation. Various methods to solve the Boltzmann equation have been developed. Among these methods, the DSMC method developed by Bird[5] is employed to solve the problem.

The simulated physical space is divided into a network of cells, and the dimensions of cell (Δx or Δy) are selected small enough to neglect the change in flow properties across each cell. Time is advanced in discrete steps of size Δt, which is small compared to the mean collision time between molecules. A large number of molecules is uniformly distributed in the computational domain, and the initial velocities of molecules are evaluated from the Maxwellian distribution function. The gas flows entering the open boundary of the computational domain are initially assumed to be an equilibrium flow and zero bulk velocity. The bulk velocity is updated by iteration, and the velocities of molecules entering the boundary are sampled from

$$f(v) = \frac{v_x}{2\pi(RT)^2 K(c_1)} \times \exp\left[-\frac{(v_x - U_1)^2 + (v_y - C_O - U_2)^2 + v_z^2}{2RT}\right] \quad (1)$$

where U_1 and U_2 are $x-$ and $y-$ component of the bulk velocity of molecules entering the open boundary, respectively, and v_x, v_y, v_z are $x-$, $y-$, $z-$ component of the velocity of molecules, and

$$K(c_1) = \exp(-c_1^2) + \sqrt{\pi}\, c_1 [1.0 + erf(c_1)] \quad (2)$$

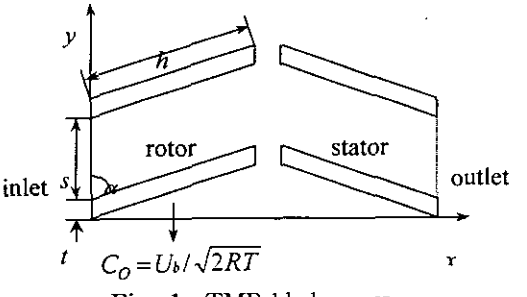

Fig. 1 TMP blade rows.

in which *erf* is the error function, and $c_1(=U_1/\sqrt{2RT})$ is the velocity ratio.[6]

When the boundary conditions (Maxwellian velocity distributions at the inlet and outlet of a blade row and diffuse reflection at the blade surfaces) have been established, the numerical simulation can be divided into the two separate procedures, i.e., free molecular motion and intermolecular collision process.

The simulation of molecular motions during Δt is carried out by disregarding intermolecular collisions. For each of simulation, molecules existing in the computational domain at time t are moved to a new positions corresponding to the free motion during Δt. The time increment Δt of collisionless motion is defined by

$$\Delta t = 0.1 \times \frac{Kn \cdot s}{\sqrt{8RT/\pi}} \tag{3}$$

in which $Kn(=\lambda/L)$ is the Knudsen number, and s is the blade spacing. To assure the accurate results in DSMC calculations, the time increment Δt is taken as $\Delta t \ll \tau$, where τ denotes the mean collision time between molecules. In the definition of Kn, the mean free path λ is derived from the mean pressure of the inlet and outlet of the blade rows, and the characteristic length L is the blade spacing s.

If a molecule collides with the blade surface, a new reflected velocity is assigned by the surface boundary condition (diffuse reflection model). The wall and the gas molecules passing through the blade rows are assumed to be an isothermal state, and molecular model is a hard sphere for simple gas.

In this study, one- and three-stage in the transition region are also analyzed to show the effects of leakage flow (through the clearance between rotor and stator) and of non-Maxwellian velocity distribution between blade rows. In the case of one- and three-stage, the last blade row (i.e., stator) faces to the outlet side of TMP. The computational grids for the three-stage are shown in Fig. 2.

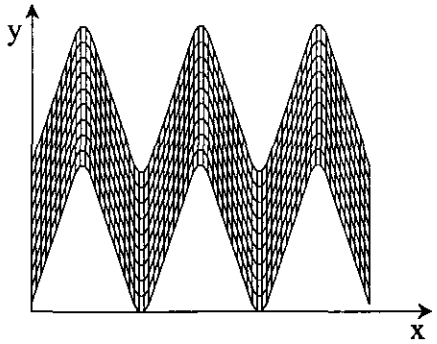

Fig. 2 Computational cells for three-stages of TMP.

2.2 Calculations of the compression ratio and pumping speed

In the process of simulation, the flow field is allowed to be developed with time. When the steady state is reached, the sampling of the molecules are started. The criterion for reaching a steady state is that the change in the relative difference between the transmission probability passing through the outlet (P_{12}) and that passing through the inlet (P_{21}) should be less than 0.1%, as marching time step Δt:

$$\frac{(P_{12}-P_{21})^t-(P_{12}-P_{21})^{t-\Delta t}}{(P_{12}-P_{21})^t} \leq 0.001 \tag{4}$$

where the superscripts t and $t-\Delta t$ denote the present time and the previous time before Δt, respectively.

For a steady state flow, the pressure increases toward the outlet and the maximum compression ratio (K_{max}) is defined by

$$K_{max}|_{Q=0} = \frac{N_{outlet}}{N_{inlet}} \tag{5}$$

in which N_{inlet} is the number of sampled molecules for the inlet side and N_{outlet} is the number of sampled molecules for the outlet side, and Q is the pumping speed.

The pumping speed has its maximum value when the inlet pressure P_{in} is equal to the outlet pressure P_{out}. The maximum pumping speed (w_{max}) is calculated by

$$w_{max} = \frac{N_{12} - N_{21}}{N_1} \tag{6}$$

in which N_{12} is the fraction that molecules coming from the inlet will ultimately reach the outlet, N_{21} is the fraction that molecules coming from the outlet will ultimately reach the inlet, and N_1 is the number of molecules coming from the inlet during sampling time.

3. Results and discussion

Numerical analyses for the performance of a TMP in both molecular and transition regions are performed over a wide pressure range. The maximum compression ratio (K_{max}) and pumping speed (w_{max}) for the single blade row and multi-stage are obtained. When the simulation program is started, gas molecules begin to move into the computational domain through the open boundaries (inlet and outlet of the blade row), and the flow field is developed with time. At first, the number of simulated molecules within the computational domain increases continuously. But, it comes to fluctuate about a certain level as the flow approaches the steady state.

Contours of molecular density distribution of the single blade row at the outlet pressure $P_2 =$ 0.5 Pa for $\alpha = 20°$, $s = 10$ mm, $h = 20$ mm, and $C_O = 0.3$ are illustrated in Fig. 3(a). According to the well known free molecular theory, most of the molecules incident on the blade row from the inlet side pass through the blade channel, but most of the molecules incident on the blade row from the outlet side are blocked by the upper blade surface. Namely, the net number of molecules transmitting ultimately through the blade channel from the inlet to the outlet is more than the reverse during the constant motion of the blades. Thus, the molecular density increases toward the outlet. As it is

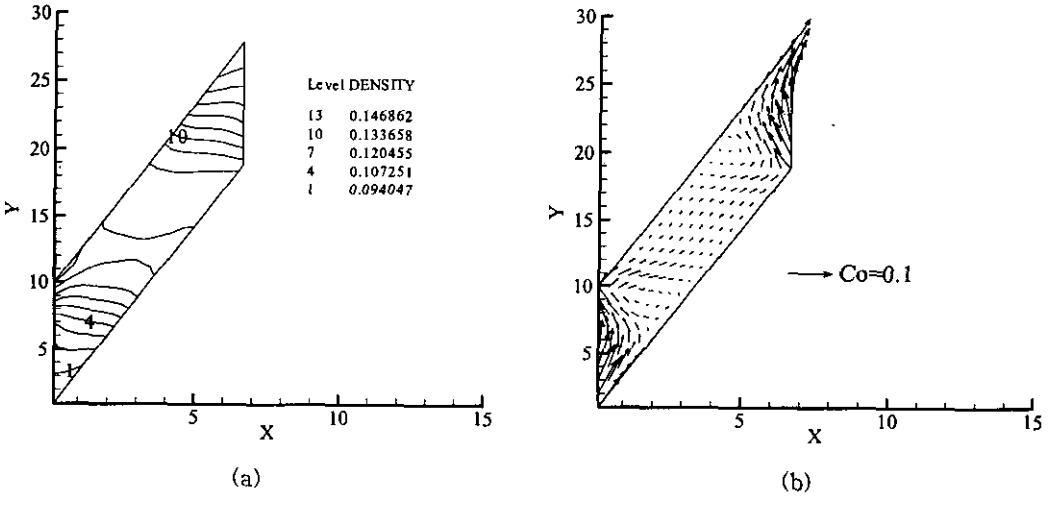

Fig. 3 (a) Density and (b) vector distributions along single blade passage for $\alpha = 20°$, $s = 10$ mm, $h = 20$ mm, and $C_O = 0.3$.

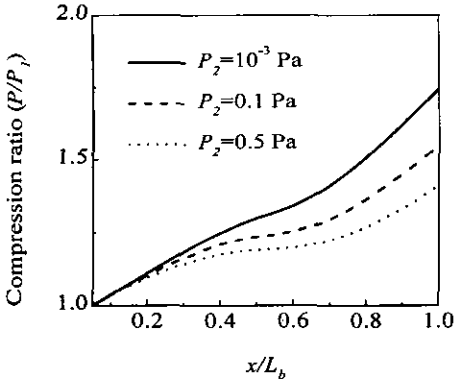

Fig. 4 Compression ratio along single blade passage for α=20°, s=10 mm, h=20 mm, and C_O=0.3.

observed clearly from the present result of DSMC simulations, gas molecules are rare near the inlet and the molecular density is higher in the upper blade surface near the outlet than the other parts of the blades. Velocity vectors are also presented in Fig. 3(b).

Profiles of the compression ratio along the blade passage for the single blade row are shown in Fig. 4, which shows the variations of compression ratio at the outlet pressure P_2= 10^{-3}, 0.1, and 0.5 Pa. In this figure, L_b denotes the distance between the inlet and the outlet of blade row. The pressure increases gradually along the blade passage, and the effects of the outlet pressure on the compression ratio are seen clearly in this figure. When the outlet pressure increases from 10^{-3} to 0.5 Pa, the compression ratio decreases by 19%.

Contours of molecular density distribution of one-stage at the outlet pressure P_2=1.0 Pa for α=20°, s=10 mm, h=10 mm, and C_O=0.3 are illustrated in Fig. 5(a). The distribution of the molecular density is continuous in the clearance region, and no sharp discontinuity is observed. Most of the molecules incident on the blade row from the outlet side are blocked by the lower blade surface of the stator. Thus, the molecular density increases toward the outlet. Velocity vectors are also presented in Fig. 5(b).

Profiles of the compression ratio along the blade passage for one-stage are shown in Fig. 6. Here, the stator faces to the outlet side of TMP. When the outlet pressure increases from 0.1 to 1.0 Pa, the compression ratio decreases by 31%. As seen in Fig. 6, gas particles are mostly compressed by the rotor. Namely, the

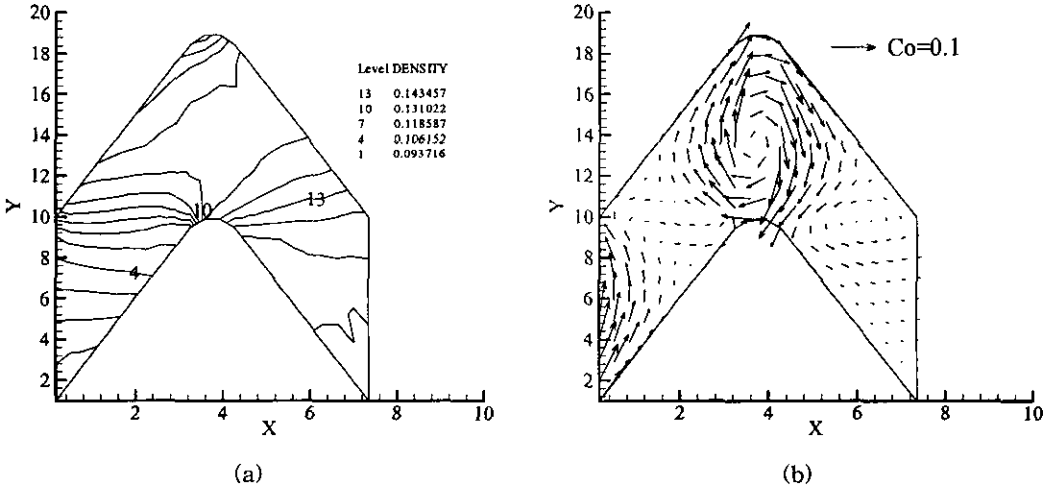

Fig. 5 (a) Density and (b) vector distributions along one-stage blade passage for α=20°, s=10 mm, h=20 mm, and C_O=0.3.

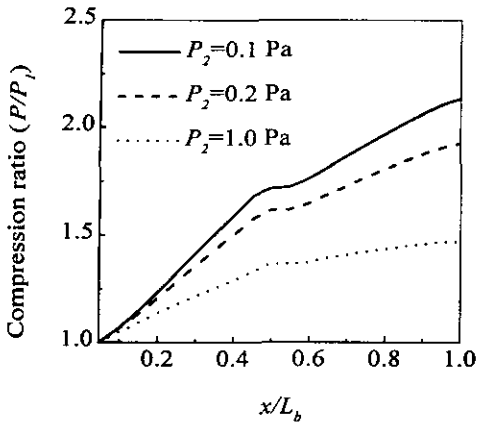

Fig. 6 Compression ratio along one-stage for $\alpha=20°$, $s=10$ mm, $h=20$ mm, and $C_O=0.3$.

role of rotor for compression is more important than that of stator. Also, the function of stator for compression is remarkably deteriorated as the outlet pressure increases. So, the stator can be omitted at the last stage of TMP. In contrast to the case of the single blade row in Fig. 4, the compression ratio in the rotor is nearly linear function of x.

Contours of molecular density distribution of three-stage at the outlet pressure $P_2=1.0$ Pa for $\alpha=20°$, $s=10$ mm, $h=10$ mm, and $C_O=0.3$ are illustrated in Fig. 7(a). Velocity vectors are also presented in Fig. 7(b).

Profiles of the compression ratio along the blade passage for three-stage are shown in Fig. 8. If the stator lies between adjacent rotors, it behaves like a rotor with an equal and opposite velocity. As seen in Fig. 8, the rate of pressure rise at the stator is comparable to that at the rotors.

In the case of single blade row, it is assumed in our analysis that the velocity distribution of molecules at each inlet and outlet side is Maxwellian. But, the velocity distribution of molecules between blade rows is, in general, not Maxwellian. To investigate the effect of non-Maxwellian velocity distributions, the new results of three-stage coupled in the analysis are compared to those obtained by using the single blade row calculations. As shown in Fig. 8, the solid circles denote the values obtained by single blade row calculations for $P_2=0.1$ Pa. The open circle represents the result for the coupled case of three-stage and rotor. Namely, in this case, the last blade row (stator) of three-stage faces not to the

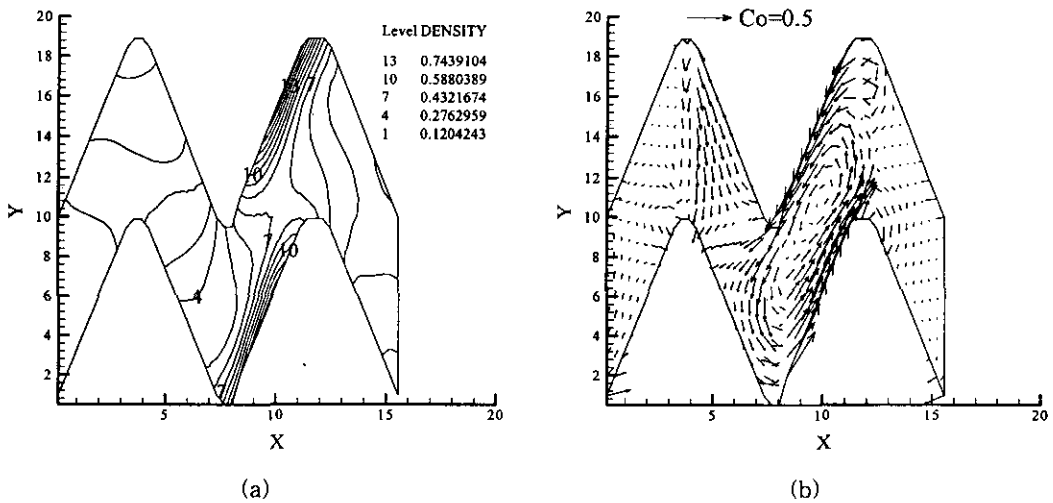

(a) (b)

Fig. 7 (a) Density and (b) vector distributions along three-stages blade passage for $\alpha=20°$, $s=10$ mm, $h=20$ mm, and $C_O=0.3$.

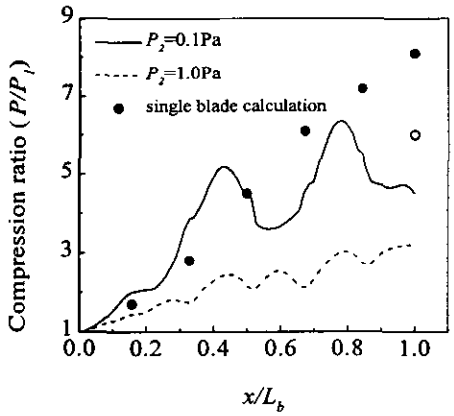

Fig. 8 Compression ratio along three-stages for $\alpha=20°$, $s=10$ mm, $h=20$ mm, and $C_O=0.3$ under the outlet pressure of 0.1 and 1.0 Pa. The open circle denotes the result for the coupled case of three-stages and rotor.

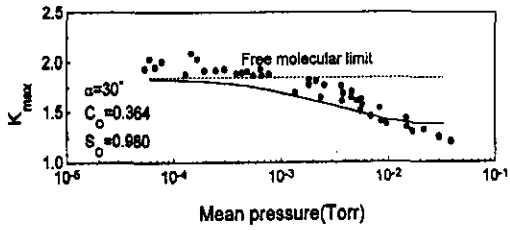

Fig. 9 Comparison of maximum compression ratio between present numerical results and experimental data.[4]

outlet of TMP but to the next blade row (rotor). The results of the single blade row provide a reasonable approximation to evaluate the compression ratio for three-stage TMP.

In the clearance region between rotor and stator, the pressure is nearly constant due to the leakage flows. In general, the measured compression ratios of a TMP are significantly lower than the calculated ones. This is mainly due to the leakage existing in the various parts of the TMP. It is noted from Fig. 6 and 8 that the leakage flowing into the clearance between rotor and stator can cause the degradation of the compression characteristics. The

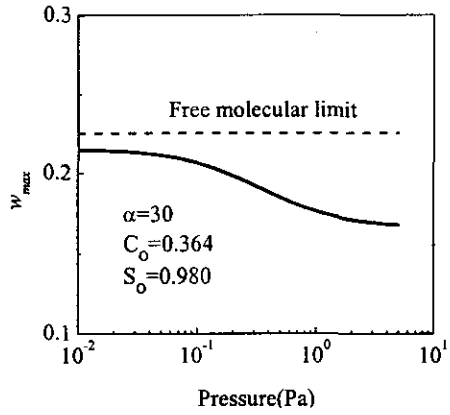

Fig. 10 Maximum pumping speed for single blade row.

effect of this leakage on the compression ratio becomes small as the outlet pressure increases.

When we compared the present numerical results for K_{max} with the previous experimental data of Sawada,[4] the numerical results agree satisfactorily with the experimental data; see Fig. 9. The dashed line in Fig. 9 is obtained by the free molecular theory ($K_{max}=1.851$). In this figure, the mean pressure is evaluated at the mean value ($=(P_1+P_2)/2$) of the inlet and outlet pressures. It is seen that K_{max} decreases as the mean pressure increases.

The value of w_{max} is plotted as a function of the pressure ($P_1=P_2$) in Fig. 10. In this figure, S_O is the spacing-chord ratio ($=s/h$). At lower pressure w_{max} becomes larger and approaches the free molecular value ($w_{max}=0.225$).

This trend for K_{max} and w_{max} is also observed in Figs. 11 and 12 for single blade row. As can be seen in these figures, K_{max} and w_{max} are strongly dependent on the Knudsen number (Kn) in the transition region, while the effect of Kn on them in the free molecular region is negligible. The reason for their reduction in the transition region is that colli-

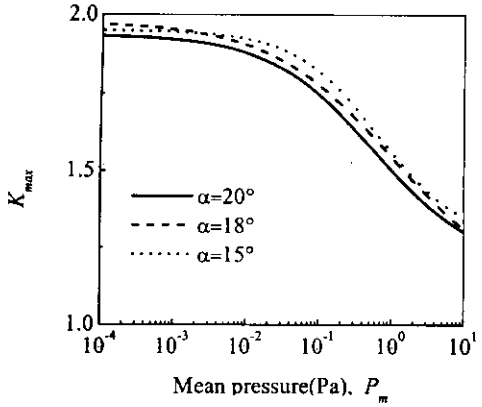

Fig. 11 Maximum compression ratio of single blade row at C_O=0.3 and S_O=0.5 for various blade angles α=20°, 18° and 15°.

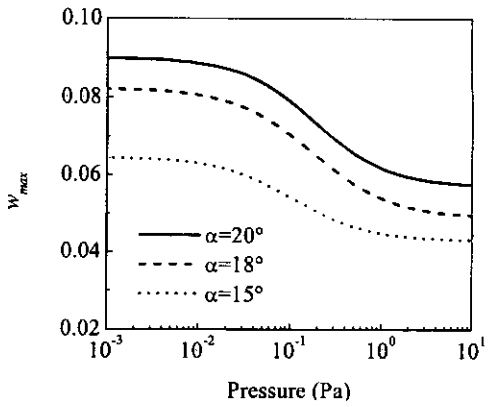

Fig. 12 Maximum pumping speed of single blade row at C_O=0.3 and S_O=0.5 for various blade angles α=20°, 18° and 15°.

sions between molecules occur so frequently, as the pressure increases, that the net number of molecules transmitting through the blade channel is greatly reduced. As a consequence, the pumping performance is remarkably deteriorated. It is of particular interest, as seen in Fig. 11, that K_{max} for α=15° becomes larger than that for α=18° at $P_m \geq 10^{-2}$ Pa.

When the gas flow is free molecular, the gas flow inside the TMP is unaffected by the back-pressure. If the back-pressure is increased, then the flow near the outlet of the TMP is not free molecular. Therefore, the gas flow or the transmission probability becomes dependent on the collisions with the back-streaming gas flow or the back-pressure.

The compression ratio as a function of the backing pressure at C_O=0.3 is plotted in Fig. 13. A commercial TMP generally consists of three or four kinds of blade. In this study, the theoretical design of a TMP which has three kinds of blade with 24-rows is made, and the compression ratio is predicted by using the single blade row results. The equations of the performance curves for a single blade are firstly obtained by curve fitting techniques (CFT) with various blade angle, and then the upstream pressure is calculated by the equations. Finally, the ultimate pressure and compression ratio are obtained by the sequential procedures. The specifications of the multi-stage TMP are given in Table 1, and the blade angle α and spacing-chord ratio S_O are arbitrarily selected similar to a commercial TMP. In each case, the compression ratio in free molecular region is about 5×10^5. But, the compression ratio obtained by CFT is larger than 5×10^5, as can be seen in Fig. 13. The difference of compression ratio between free mo-

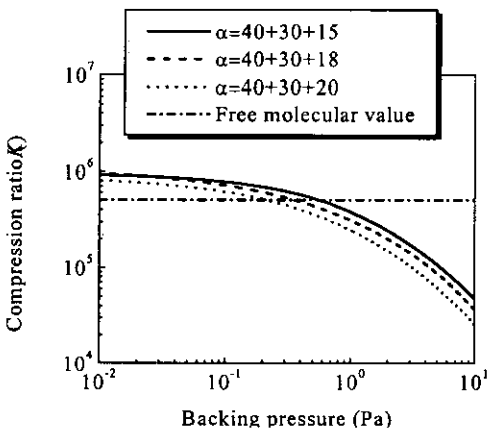

Fig. 13 Variation of compression ratio with backing pressure.

Table 1 Specification of multi-stage TMP

Blade row	1~4	5~14	15~24
α	40°	30°	20°, 18°, 15°
S_O	1.0	1.0	0.5

lecular value and present ones obtained by CFT is due to the absence of the stator correction steps originated by Kruger and Shapiro.[7]

Evidently, to predict correctly the performance of a multi-stage TMP, the DSMC method must be applied to the entire set of blade rows. Since a normal TMP consists of several tens or more stages, however, the more computational efforts and higher expenses are required to employ the DSMC method. If the single blade row calculations give reasonable results, this approximation method might be very useful. As mentioned above, it is possible to approximate the pumping performance reasonably by using the single blade results.

4. Conclusions

The performance of a TMP in both molecular and transition flow regions is numerically predicted by using the direct simulation Monte Carlo method. For a single blade row, it is found that the calculated results agree well with the previous experimental data. Some major conclusions from this study are as follows.

The dimensionless, maximum-compression ratio (K_{max}) and pumping speed (w_{max}) decrease significantly as the operating pressure increases. The values of K_{max} and w_{max} are strongly dependent on the Knudsen number (Kn) in the transition region, while the effect of Kn on them in the free molecular region is very small. This is due to the fact that collisions between molecules occur so frequently, as the pressure increases, that the net number of molecules transmitting through the blade channel is greatly reduced.

In the last stage of TMP, the stator function for the compression is remarkably deteriorated as the outlet pressure increases, and most of the gas compression is achieved in the rotor. However, if the stator lies between adjacent rotors, it behaves like a rotor with an equal and opposite velocity and the rate of pressure rise at the stator is comparable to that at the rotors. The leakage flowing into the clearance between rotor and stator can cause the degradation of the compression characteristics, and the effect of this leakage on the compression ratio becomes small as the outlet pressure increases. The overall compression ratio through the entire stages in both molecular and transition regions is calculated by using the curve fitting techniques and the calculated results agree well with the compression ratio predicted by the free molecular theory.

Acknowledgement

This work was supported by grant No. 2000-1-30400-014-3 from the Basic Research Program of the Korea Science and Engineering Foundation.

References

1. Hablanian, M. H., 1990, High-Vacuum Technology (A Practical Guide), Marcel Dekker, Inc.
2. Hablanian, M. H., 1994, In Vacuum Science and Technology: Pioneers of 20th Century, edited by P. A. Redhead (AIP, New York), pp. 126-132.
3. Sawada, T., 1973, The Axial Flow Molecular Pump, Bull. JSME, Vol. 16, No. 96, pp. 993-1001.
4. Sawada, T., 1979, Performance of a Turbomolecular Pump in the Transition and Slip Flow Regimes, Bull. JSME, Vol. 22, No. 165, pp. 362-369.
5. Bird, G. A., 1994, Molecular Gas Dynamics

and the Direct Simulation of Gas Flows, Clarendon Press, Oxford.

6. Nanbu, K., Kubota, H., Igarashi, S., Urano, C. and Enosawa, H., 1991, Performance of Spiral Grooves on a Rotor of Turbomolecular Pump, Trans. JSME, Vol. 57, No. 533, pp. 172-177.
7. Kruger, C. H. and Shapiro, A. H., 1961, In Rarefied Gas Dynamics, edited by L. Talbot (Academic Press, New York), pp. 117-140.